Titration and Exchange Studies of Liver Fatty Acid-Binding Protein with ^{13}C-Labeled Long-Chain Fatty Acids†

Hsin Wang,‡ Yan He,‡ Christopher D. Kroenke,§ Sarala Kodukula,|| Judith Storch,*,|| Arthur G. Palmer,§ and Ruth E. Stark*,‡

Department of Chemistry, CUNY Graduate Center and College of Staten Island, 2800 Victory Boulevard, Staten Island, New York 10314, Department of Nutritional Sciences, Cook College, Rutgers University, New Brunswick, New Jersey 08901, and Department of Biochemistry and Molecular Biophysics, Columbia University, 630 West 168th Street, New York, New York 10032

Received October 10, 2001; Revised Manuscript Received February 21, 2002

ABSTRACT: Uniformly ^{13}C-labeled long-chain fatty acids were used to probe ligand binding to rat liver fatty acid-binding protein (LFABP), an atypical member of the fatty acid-binding protein (FABP) family that binds more than one molecule of long-chain fatty acid, accommodates a variety of diverse ligands, and exhibits diffusion-mediated lipid transport to membranes. Two sets of ^{1}H−^{13}C resonances were found in a titration series of NMR spectra for oleate−LFABP complexes, indicating that two molecules of the fatty acid are situated in the protein cavity. However, no distinct resonances were observed for the excess fatty acid in solution, suggesting that at least one ligand undergoes rapid exchange with oleate in the bulk solution. An exchange rate of 54 ± 6 s^{-1} between the two sets of resonances was measured directly using ^{13}C *z*,*z*-exchange spectroscopy. In light of these NMR measurements, possible molecular mechanisms for the ligand-exchange process are evaluated and implications for the anomalous fatty acid transport mechanism of LFABP are discussed.

Liver fatty acid-binding protein (LFABP)[1] belongs to a family of intracellular lipid-binding proteins (FABPs) that have long been hypothesized to participate in cellular fatty acid trafficking, regulation of lipid metabolism, and protection from fatty acid cytotoxicity (*1*). The mammalian FABP family is composed of more than 10 separate gene products. Each of the proteins displays a unique tissue distribution, and more than one FABP form can be expressed simultaneously in a single cell type. Consequently, distinct functional roles have been inferred for individual FABPs. The structures of the 14−15 kDa FABPs feature a pair of nearly orthogonal five-stranded β-sheets and a short helix−turn−helix motif between strands βA and βB (*2*). The lipid binding cavity is formed between the two β-sheets.

LFABP is notable within the family of FABPs in three respects. First, the lipid-binding cavity of LFABP accommodates more than one fatty acid molecule (*2*−*4*). Second, LFABP has been reported to bind not only long-chain fatty acids but also diverse ligands including acyl-CoA esters, bile salts, lysophopholipids, monoacylglycerol, cholesterol, cyclopentenone prostaglandins, bilirubin, and hemes (*1*, *5*−*7*). Third, whereas most other FABPs transfer fatty acids to and extract lipids from model membranes via direct protein−membrane collisions, LFABP has an atypical aqueous diffusion-mediated lipid transfer mechanism (*8*, *9*).

The molecular structure of LFABP in complex with oleate (OLA) has been determined by X-ray crystallography (*10*). One bound oleate molecule (OLA 129) lies deep within the cavity, inaccessible to solvent. Its carboxylate group is involved in an extensive hydrogen-bonding network that includes the side chains of R122, S39, and S124 and possibly bound water molecules. A second oleate molecule (OLA 128) fills the remainder of the cavity; its ω-methyl group is deeply buried, and its carboxylate moiety lies near the surface and is exposed to solvent. This latter position is similar to, but has an orientation opposite of, that of the bound ligands in other FABPs. In addition to the two well-defined bound fatty acids, electron density for a four-carbon segment was observed near the outer surface of the protein's first helix. That fragment was hypothesized to be part of a third oleate molecule, for which the remainder was too flexible to be resolved in the X-ray structure (*10*).

Biochemical and spectroscopic studies have reported varying fatty acid binding stoichiometries between 1 and 8 for LFABP (*11*, *12*). We have recently found that [^{15}N]-LFABP can be titrated with 6−8 equiv of oleate before any precipitation is observed (Y. He et al., unpublished experiments).

These biochemical, spectroscopic, and crystallographic results suggest that the recognition of ligands by LFABP is more complex than previously appreciated and that the

† This work was supported by grants from the National Institutes of Health (DK38389 and GM59273) and the Professional Staff Congress of CUNY (69181 and 61209). Operation of the NMR facility was supported by the CUNY Center for Applied Biomedicine and Biotechnology and the College of Staten Island. A.G.P. and R.E.S. are Principal Investigators of the New York Structural Biology Center.

* To whom correspondence should be addressed. Phone: (718) 982-3894. Fax: (718) 982-4077 or (718) 982-3910. E-mail: stark@postbox.csi.cuny.edu.

‡ CUNY Graduate Center and College of Staten Island.

§ Columbia University.

|| Rutgers University.

[1] Abbreviations: FABP, fatty acid-binding protein; LFABP, liver fatty acid-binding protein; FA, fatty acid; PA, palmitic acid; OLA, oleic acid.

10.1021/bi011914g CCC: $22.00
Published on Web 03/30/2002

distinctive FA transport mechanism of LFABP may arise in part from its unique ligand binding properties. In the studies presented here, NMR spectroscopy has been used to characterize the binding of uniformly ^{13}C-labeled long-chain fatty acids to LFABP. Sites at both ends of palmitic and oleic fatty acid molecules (terminal ω-methyl, α-methylene, and carboxyl carbons) yielded well-resolved resonances, distinct from interior methylene chain moieties. These resonances were used to probe binding site occupancy, ligand environments, and binding kinetics. These observations afford new insights into the binding and transport properties of this intracellular protein.

EXPERIMENTAL PROCEDURES

Materials for NMR Studies. Uniformly ^{15}N-enriched rat liver FABP samples were produced as described previously (*13*). Protein solutions were prepared in a pH 7.0 phosphate buffer containing 50 mM Na_2HPO_4/NaH_2PO_4, 100 mM NaCl, 50 μM EDTA, 0.02% NaN_3, and a 95% H_2O/5% D_2O mixture.

Preparation of [U-^{13}C]Palmitate-Bound LFABP. [U-^{13}C]-Palmitic acid (PA, 16:0) was purchased as the free acid from Cambridge Isotope Laboratories (Andover, MA). Due to the low solubility of the saturated fatty acid (*14*), the PA−LFABP complex was prepared initially in dilute basic solution to ensure complete binding. A 900 μL sample of 0.46 mM [U-^{15}N]LFABP was eluted through a PD-10 gel filtration column (Pharmacia, Piscataway, NJ) with 100 mM $(NH_4)_2CO_3$ at pH 9.5 and then mixed with 5 mL of 0.25 mM [U-^{13}C]palmitate at pH 9.6 to obtain a ligand-to-protein ratio of 3:1. The mixture was stirred overnight at 4 °C and then subjected sequentially to the following treatments: (a) ultrafiltration (Centricon-10 column from Millipore, Bedford, MA) with 100 mM $(NH_4)_2CO_3$ to remove any unbound fatty acid, (b) PD-10 gel filtration to exchange the solvent with pH 7.0 phosphate buffer, and (c) ultrafiltration with pH 7.0 phosphate buffer to reduce the volume. The final protein concentration was assayed at 0.73 mM (*15*, *16*).

Titration of LFABP with [U-^{13}C]Oleate. [U-^{13}C]Oleic acid (OLA, 18:1) was purchased as the free acid from Isotec (Miamisburg, OH). The higher solubility of oleic acid permitted preparation of a stock solution of 10 mM [U-^{13}C]-OLA after the acid was neutralized with NaOH at pH 9.6. Aliquots of this stock solution were titrated directly into a 550 μL sample of 0.26 mM [U-^{15}N]LFABP in pH 7.0 phosphate buffer, producing holoprotein samples with ligand-to-protein molar ratios of 0.5:1, 1:1, 1.5:1, 2:1, 3:1, and 4:1. The addition of unbuffered sodium oleate (pH 9.6) did not alter the pH of the protein solution. The protein concentrations were measured before the addition of ligand using a corrected Lowry method (*15*) and/or absorption at 280 nm (*16*).

NMR Experiments. Unless otherwise stated, data were collected on a four-channel Varian ^{UNITY}INOVA 600 MHz spectrometer (Varian NMR Inc., Palo Alto, CA) equipped with a triple-resonance probe and *z*-axis pulsed field gradients. In all experiments, the ^{1}H carrier frequency was placed on resonance with the H_2O signal.

^{13}C spectra of [U-^{13}C]oleate-bound [^{15}N]LFABP and [U-^{13}C]palmitate-bound [^{15}N]LFABP were obtained with one-dimensional (1D) ^{13}C NMR, two-dimensional (2D) ^{13}C HSQC, constant-time ^{13}C HSQC (*17*), and HCACO experiments (*18*) between 5 and 35 °C. The HSQC data were acquired with 160 complex points in t_1, 512 complex points in t_2, and the WET scheme (*19*) for water suppression. The ^{13}C carrier frequency was placed at 30 ppm for the PA−LFABP complex, and at 80 ppm for the OLA−LFABP complex to improve the observation of resonances associated with the fatty acid double bond. The spectral widths in the ^{1}H and ^{13}C dimensions were 7500 and 9052 Hz, respectively. 2D versions of the CT-HCACO experiment were used to obtain HA−CA and HA−CO chemical shift correlations. The ^{13}C carrier frequency was placed at 35 ppm, and ^{13}CO pulses were generated by 21 kHz downfield-shifted laminar pulses (*20*). Spectra were acquired with 64 complex points and a 3000 Hz spectral width in the Cα dimension and with 64−90 complex points and a spectral width of 1800 Hz in the CO dimension.

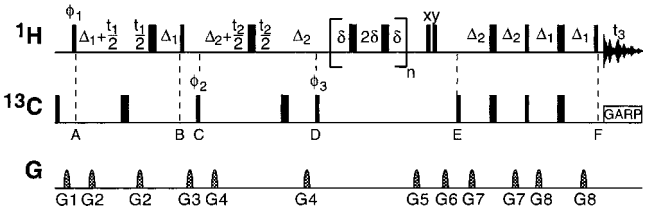

FIGURE 1: Pulse sequence for the *z*,*z*-exchange experiment. Narrow and wide bars depict 90° and 180° pulses, respectively. All pulses are of *x* phase unless otherwise indicated. Water suppression was achieved using presaturation during the 1 s recycle delay. Decoupling during the acquisition period used the GARP sequence (*41*). The *xyz*-gradients are indicated by hatched bars and were used for suppression of artifacts and the residual water signal (*42*). The delays are as follows: $\Delta_1 = 1.25$ ms, $\Delta_2 = 0.75$ ms, and $\delta = 2.5$ ms. The bracketed sequence of pulses and delays was repeated *n* times. Delays t_1, t_2, and t_3 are indirect ^{1}H, indirect ^{13}C, and direct ^{1}H (acquisition) frequency labeling periods, respectively. The effective mixing period during which magnetization exchange takes place, τ_m, corresponds to the time between points B and F and was varied through changes in the value of *n*. Pulse phases are as follows: $\phi_1 = x, -x$; $\phi_2 = x, x, -x, -x$; $\phi_3 = y, y, y, y, -y, -y, -y, -y$; and receiver $= x, -x, -x, x, -x, x, x, -x$. Quadrature detection was obtained using States−TPPI phase cycling (*43*) of ϕ_1 and ϕ_2 for t_1 and t_2, respectively.

Chemical exchange of the ^{13}C-enriched oleate molecules in the 4:1 stoichiometric complex was monitored at 10 °C using ^{13}C *z*,*z*-exchange spectroscopy (*21*−*23*) on a four-channel Bruker DRX 600 MHz spectrometer (Bruker Instruments, Billerica, MA) equipped with a triple-resonance probe and *x*,*y*,*z*-axis pulsed field gradients. The pulse sequence shown in Figure 1 is similar to previously published methods (*21*), but an additional frequency labeling period is used to resolve oleate α-methylene and ω-methyl hydrogen resonances from other methylene signals. A refocused INEPT period spans points A−D in Figure 1, with ^{1}H frequency labeling occurring between points A and B and ^{13}C frequency labeling between points C and D. Transverse ^{13}C coherence is converted to longitudinal magnetization at point D, and a variable delay follows until point E. Points E and F demarcate another refocused INEPT period that converts ^{13}C magnetization back to ^{1}H for detection. NMR data were acquired with spectral widths of 2803, 3205, and 10 000 Hz and 32, 16, and 1024 complex points in the t_1, t_2, and t_3 dimensions, respectively. A total of 128 transients were recorded per (t_1, t_2) complex pair. The ^{1}H carrier frequency was resonant with the water signal, and the ^{13}C carrier frequency was set to

26.1 ppm. Chemical exchange that occurs during the time between points B and F results in signal intensity changes as a function of the variable delay, because affected nuclei precess at different frequencies during periods t_1, t_2, and t_3. The spectra were acquired with exchange delays, τ_m, of 10.7, 21.9, 31.9, 61.9, 111.9, 211.9, and 511.9 ms, including the magnetization transfer periods between points B and F, but not including t_2. To minimize the effects of exchange during t_2, the maximum value of t_2 (4.99 ms) was kept as short as possible to ensure that exchange kinetics are $\ll 1/t_{2max}$.

NMR Data Processing. Except as noted below for the *z,z*-exchange experiments, all NMR spectra were processed with NMRPipe (*24*) and analyzed with the NMRView program (*25*). The ^{13}C HSQC time domain data for the PA−LFABP complex were multiplied by an 81°-shifted sine bell-squared weighting function in t_2 and a 90°-shifted sine bell-squared weighting function in t_1. HSQC data in the oleate titration series were apodized using Lorentz-to-Gauss transformations in both the t_2 and t_1 dimensions with exponential broadening of −7 and −10 Hz, respectively, Gaussian broadening of 20 and 40 Hz, respectively, and an offset factor of 0.1 for the Gaussian maximum. After zero filling and Fourier transformation, the resulting matrices had 1024 × 512 points. For oleate titrations, peak volumes were obtained from ^{13}C HSQC spectra using the nonlinear line shape modeling routine *nlinLS* of the NMRPipe program with Gaussian line shape modeling in both dimensions. The peak volumes were then adjusted assuming logarithmic scaling of signal amplitude according to the value of the receiver gain.

The *z,z*-exchange data were processed using Felix 97 (MSI, San Diego, CA). The spectra were processed using a Lorentz-to-Gauss window function (exponential broadening of −20 Hz, Gaussian broadening of 30 Hz) in the direct dimension, and Kaizer windows with arguments of 32 and 16 in the indirect ^{1}H and ^{13}C dimensions, respectively. Signal intensities were estimated as the sum of three intensity values along the direct-detect frequency axis, centered on the peak maximum. Peak volumes were estimated using standard Felix software routines. For each time point, four peaks are observed with intensities denoted by $I_{AA}(\tau_m)$, $I_{BA}(\tau_m)$, $I_{BB}(\tau_m)$, and $I_{AB}(\tau_m)$ for the upper right, upper left, lower left, and lower right peaks in the spectra, respectively. For exchange between two sites A and B, the intensities of the autocorrelation resonances, $I_{AA}(\tau_m)$ and $I_{BB}(\tau_m)$, and of the cross-peaks, $I_{BA}(\tau_m)$ and $I_{AB}(\tau_m)$, are governed by the relations (*21*−*23*)

$$I_{AA}(\tau_m) = I_{AA}(0)[p_A + p_B \exp(-k_{ex}\tau_m)] \exp(-R_1\tau_m)$$

$$I_{BB}(\tau_m) = I_{BB}(0)[p_B + p_A \exp(-k_{ex}\tau_m)] \exp(-R_1\tau_m)$$

$$I_{BA}(\tau_m) = I_{AA}(0)p_B[1 - \exp(-k_{ex}\tau_m)] \exp(-R_1\tau_m)$$

$$I_{AB}(\tau_m) = I_{BB}(0)p_A[1 - \exp(-k_{ex}\tau_m)] \exp(-R_1\tau_m) \quad (1)$$

in which the p_i values are relative populations for sites i, k_{ex} is the sum of the forward, k_1, and reverse, k_{-1}, kinetic rate constants for interconversion between sites, and R_1 is the longitudinal relaxation rate of the ^{13}C nucleus in the spin system. The R_1 values are assumed to be equal for both magnetic environments of an interconverting pair. The total cross-peak volume $[I_{BA}(\tau_m) + I_{AB}(\tau_m)]$ for each time point, τ_m, was fit to the sum of the third and fourth equalities given in eq 1 to obtain k_{ex} and R_1. The relative populations p_A and p_B were determined from cross-peak volumes of a ^{13}C HSQC spectrum obtained using a 7.5 s recycle delay to ensure the restoration of equilibrium magnetization between transients.

Molecular Structures. Coordinates for graphical representations of IFABP and LFABP were obtained from Protein Data Bank entries 2ifb (*26*) and 1lfo (*10*), respectively, and displayed with the SYBYL program (Tripos Associates, St. Louis, MO).

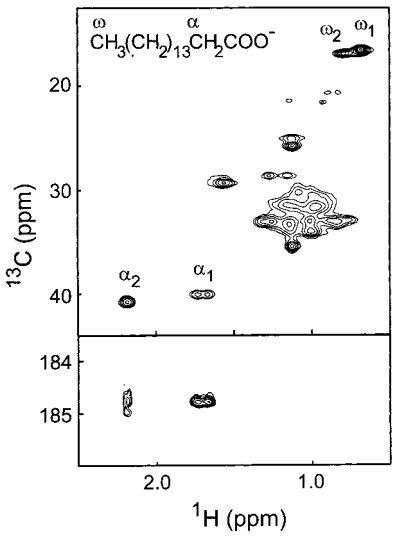

FIGURE 2: ^{13}C NMR of a complex of [U-^{13}C]palmitate (PA) and liver fatty acid-binding protein. PA is bound to [U-^{15}N]LFABP at a mole ratio between 2:1 and 3:1 at pH 7 and 10 °C. The top panel shows the ^{13}C HSQC spectrum and the bottom panel the H_α−CO correlation spectrum measured with a 2D CT-HCACO experiment. Proton and carbon chemical shifts were referenced to external DSS.

RESULTS

Ligand Environments for LFABP-Bound Palmitate (PA). NMR spectra for protein-bound palmitate in the PA−LFABP complex, acquired at 10 °C to enhance the spectral resolution, are displayed in Figure 2. Two sets of resonances are evident in the ^{13}C HSQC correlation spectra for both ω-methyl and α-methylene groups of the fatty acid ligands (top panel), indicating two ligand electronic environments in slow exchange. In addition, one α-methylene group (labeled α_1) has distinct prochiral protons with a chemical shift dispersion of 0.07 ppm. This latter difference in magnetic environment is roughly $^1/_{10}$ the size of that reported, for instance, in the PA−HFABP complex (*27*). Despite the expected sensitivity of carboxyl carbon chemical shifts to the electronic environment, the HCACO experiment shows that the two PA molecules have nearly degenerate ^{13}CO resonances (bottom panel). The coupled ^{13}C spectrum confirms this similarity, showing one doublet with a $^1J_{CC}$ splitting of 49.0 Hz (data not presented).

Ligand Environments for LFABP-Bound Oleate (OLA). The 4:1 OLA−LFABP preparation has spectroscopic properties very similar to those of the PA−LFABP holoprotein, in terms of both the protein backbone ^{15}NH chemical shift fingerprint (Figure 3) and the fatty acid ^{1}H and ^{13}C chemical shifts (Figure 4). In contrast to the results for the PA−LFABP complex, however, the CT-HCACO experiment with the OLA−LFABP complex reveals two distinct ^{13}CO resonances

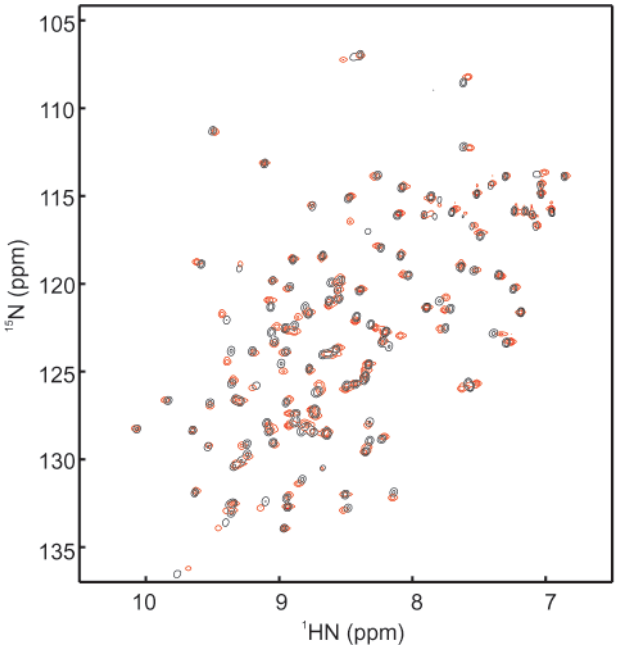

FIGURE 3: ^{15}N NMR of LFABP complexed with two different fatty acids. ^{15}N HSQC spectra are displayed for [U-^{15}N]LFABP bound to two PA molecules (red) and to four OLA molecules (black). Residue F3 displays ^{1}H−^{15}N cross-peaks at 11.31 and 131.8 ppm (PA complex) and at 11.50 and 131.8 ppm (OLA complex) (data not shown). Site-specific spectral assignments, along with analyses of chemical shift and line width perturbations, will appear elsewhere (Y. He et al., unpublished experiments).

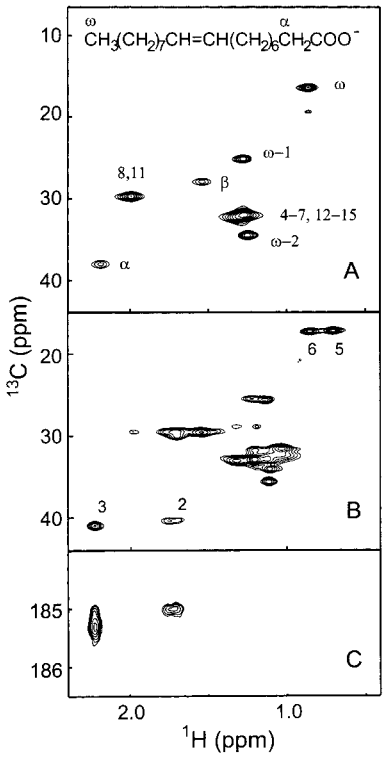

FIGURE 4: ^{13}C NMR of oleate (OA) complexed to liver fatty acid-binding protein. A 4:1 complex of [U-^{13}C]oleate (OLA) is bound to 0.26 mM [U-^{15}N]LFABP at pH 7 and 10 °C. (A) ^{13}C HSQC spectrum of a freshly prepared 2 mM oleate suspension (no protein present) at pH 7 and 10 °C, measured with a relaxation delay of 1.5 s and assigned using a ^{13}C HMQC-TOCSY experiment. (B) ^{13}C HSQC spectrum acquired with a relaxation delay of 1.5 s. (C) H_α−CO correlation spectrum measured with a 2D CT-HCACO experiment. To rule out the possibility that NMR signals from slowly relaxing free OLA molecules are attenuated, similar spectral results were verified from HSQC experiments conducted with a relaxation delay of 7.5 s (data not shown). The olefinic proton resonances are obscured by water.

with a separation of 0.2 ppm (30 Hz). If these resonances correspond to the oleate molecules at different sites within the protein cavity (*10*), then their exchange rate constant is smaller than the chemical shift difference at this field strength (∼190 s^{-1}, Figure 4B). Of the two sets of resonances in the α-CH_2 and *ω*-CH_3 regions, peaks 3 and 6 have ^{1}H chemical shifts similar to those observed in a fresh (slightly opaque) 2 mM oleate suspension at the same pH (Figure 4A). Furthermore, peak 2 shows a prochiral separation of 0.03 ppm, close to that observed in the PA−LFABP complex. Thus, peaks 2 and 5 are tentatively assigned to the more tightly bound OLA molecule, which is expected to be buried more deeply within the protein cavity. The ^{13}C HSQC spectra in Figure 4 were measured on a LFABP sample containing 4 equiv of oleate. Thus, the observation of only two sets of OLA resonances, made at all accessible temperatures between 5 and 35 °C, suggests that rapid exchange processes are occurring between the bound and excess OLA molecules (see below).

Titration of LFABP with [U-^{13}C]OLA. To examine ligand binding by LFABP more closely, the growth in peak intensities was monitored by NMR spectroscopy during titration of LFABP with OLA. Figure 5 shows an overlay of the ^{13}C HSQC spectra obtained at the beginning (0.5:1 OLA:LFABP ratio, red) and end (4:1 OLA:LFABP ratio, black) of the titration. The regions highlighted by boxes contain minimally overlapped peaks that could be assigned readily by comparison with free oleate, which was assigned in turn using an HMQC-TOCSY experiment (*28*) (data not shown). The titration curves that track changes in the cross-peak volumes are plotted in Figure 6.

When the proportion of OLA is small compared to protein, resonances 1 and 4 are dominant in the α- and *ω*-carbon regions, respectively. These peaks have chemical shifts that are close to but nevertheless distinct from the deeply bound oleate molecule of the fully ligated complex (peaks 2 and 5). Thus, resonances 1 and 4 probably arise from the deeply bound oleate in the singly ligated OLA−LFABP complex. As the OLA stoichiometry increases, peaks 1 and 4 diminish in volume compared with peaks 2 and 5. At an OLA:protein ratio of 1:1, α resonances 1 and 2 are very weak and the ligand may undergo intermediate exchange between singly and doubly occupied species, because only two sets of resonances are observed for the fully occupied complex. The simplest interpretation of these results is that the LFABP protein binds at least two OLA molecules. This conclusion is consistent with the X-ray structure (*10*), ^{15}N HSQC studies of the oleate titration (Y. He et al., unpublished experiments), and protein−ligand ^{1}H−^{1}H nuclear Overhauser effects (NOEs) (X.-M. Yang et al., unpublished experiments). The fact that no resonances can be attributed solely to the excess bulk oleate suggests that free and bound oleate molecules are in rapid chemical exchange.

Exchange Processes for Both Bound OLA Sites. The second OLA molecule entering the binding cavity can exchange rapidly on the NMR time scale with bulk oleate, resulting in a set of averaged resonances for both bound and free species. An analogous exchange phenomenon was not

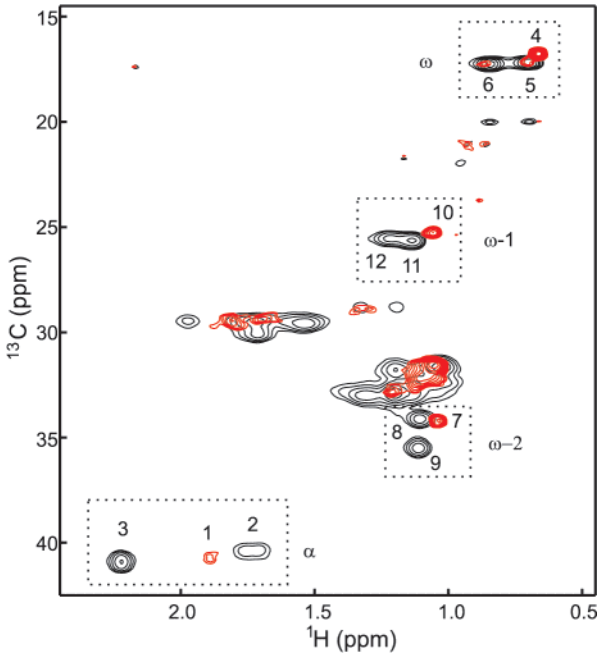

FIGURE 5: ^{13}C NMR spectra during titration of liver fatty acid-binding protein with OLA. ^{13}C HSQC spectra are compared at the beginning (0.5:1 OLA:LFABP ratio, red) and end (4:1 OLA:LFABP ratio, black) of the titration.

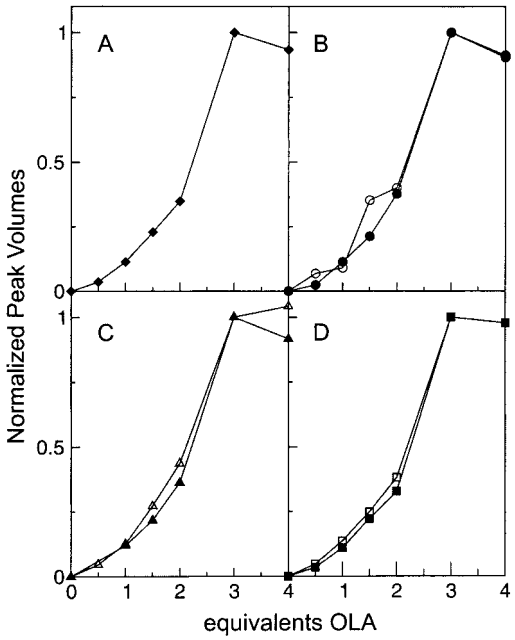

FIGURE 6: Growth in ^{13}C HSQC cross-peak volumes of several OLA resonances during the course of titration into LFABP solution: (A) α-carbon (peak 3 in Figure 5), (B) ($\omega-2$)-carbons (peaks 8 and 9), (C) ($\omega-1$)-carbons (peaks 11 and 12), and (D) ω-carbons (peaks 5 and 6). Volumes for each carbon type are normalized to the value measured in the presence of 3 equiv of oleate. Filled symbols represent hydrogen atoms with chemical shifts similar to those of [^{13}C]OLA in aqueous solution (L_2 site), whereas empty symbols represent internally liganded OLA (L_1 site); the seven curves are essentially superimposable. The α-carbon cross-peaks from the internal OLA (peak 2) are omitted because they are not modeled well by the nonlinear fitting routine of the NMRPIPE program. Volume variations of peaks attributed to the singly ligated complex (1, 4, 7, and 10) are also omitted for clarity.

expected for the first OLA molecule, because that ligand displays distinct NMR signals and is thought to bind more

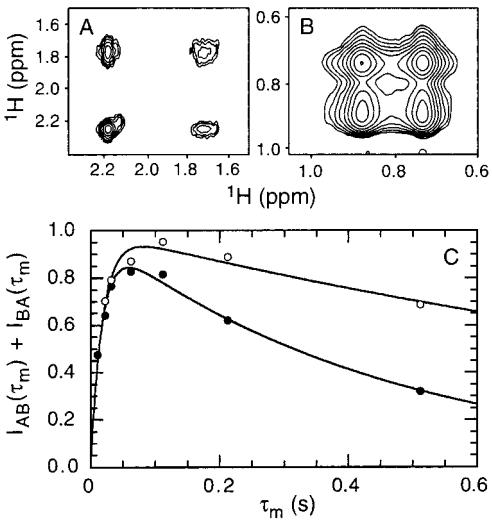

FIGURE 7: Spectra and peak intensities obtained from the *z,z*-exchange experiment. Panels A and B show regions of the ^{1}H−^{1}H plane containing the α-methylene and ω-methyl signals, respectively, obtained for a τ_m value of 61.9 ms. Panel C displays a plot of the sum of exchange peak intensities [$I_{BA}(\tau_m) + I_{AB}(\tau_m)$] vs exchange delay, τ_m, for the (○) ω-methyl and (●) α-methylene spin systems. The solid lines are the best nonlinear least-squares fits to the expression $I_{BA}(\tau_m) + I_{AB}(\tau_m) = A[1 - \exp(-k_{ex}\tau_m)] \exp(-R_1\tau_m)$, in which A is a scaling parameter. The data are normalized so that $A = 1$.

tightly within the protein cavity. Thus, according to this expectation, the intensities of peaks 3, 6, 9, and 12 (Figure 5) would continue to grow after addition of 2 equiv of OLA, whereas those of peaks 2, 5, 8, and 11 would remain approximately constant. The results shown in Figure 6 are therefore surprising: both sets of resonances and all carbon signals grow in size at essentially the same rate upon addition of 3 equiv of OLA, and their cross-peak volumes reach a plateau between 3 and 4 equiv of OLA. These observations suggest that both OLA sites are involved in rapid chemical exchange with bulk fatty acid.

Ligand Exchange Rates from ^{13}C z,z-Exchange Spectroscopy. As noted above, OLA methyl and α-methylene resonances each give rise to two resolved NMR signals in ^{1}H−^{13}C correlation spectra of the oleate ligand in the 4:1 complex, reflecting the presence of two highly populated magnetic environments. The *z,z*-exchange pulse sequence of Figure 1 was used to investigate the kinetics of the interconversion between these two sites. Displayed in Figure 7 (panels A and B) are regions of the ^{1}H−^{1}H planes for α-CH_2 and ω-CH_3 signals, recorded using a τ_m delay of 61.9 ms. For each time point, four peaks are observed with intensities denoted $I_{AA}(\tau_m)$, $I_{BA}(\tau_m)$, $I_{BB}(\tau_m)$, and $I_{AB}(\tau_m)$ for the upper right, upper left, lower left, and lower right peaks in the spectra, respectively. For the α-methylene groups, the designations A and B refer to peaks 2 and 3, respectively; for the ω-methyl groups, they refer to peaks 5 and 6, respectively. Figure 7C shows the sum $I_{BA}(\tau_m) + I_{AB}(\tau_m)$ for each time point, plotted versus τ_m. The estimates of k_{ex} and R_1 obtained from the nonlinear least-squares optimization are summarized in Table 1. As anticipated for resolved resonances, both values of k_{ex} (53 and 55 s^{-1}) were smaller than the ^{1}H chemical shift differences (570 and 1900 s^{-1}). Chemical shift differences are smaller for the ^{13}C resonances than for the ^{1}H resonances, so the exchange process is faster

Table 1: Oleate Chemical-Exchange Parameters

spin system	p_B/p_A	k_1 (s^{-1})	k_{-1} (s^{-1})	k_{ex} (s^{-1})	R_1 (s^{-1})[a]
α-methylene	1.11 ± 0.06	29.0 ± 2.9	26.1 ± 2.6	55.1 ± 5.3	2.21 ± 0.22
ω-methyl	1.49 ± 0.07	32.0 ± 4.4	21.4 ± 3.0	53.4 ± 7.2	0.70 ± 0.17

[a] The effects of differences in R_1 values for the two sites (R_{1A} and R_{1B}) are insignificant provided that $k_{ex} \gg |R_{1A} - R_{1B}|$. In the case presented here, the inequality is well-satisfied.

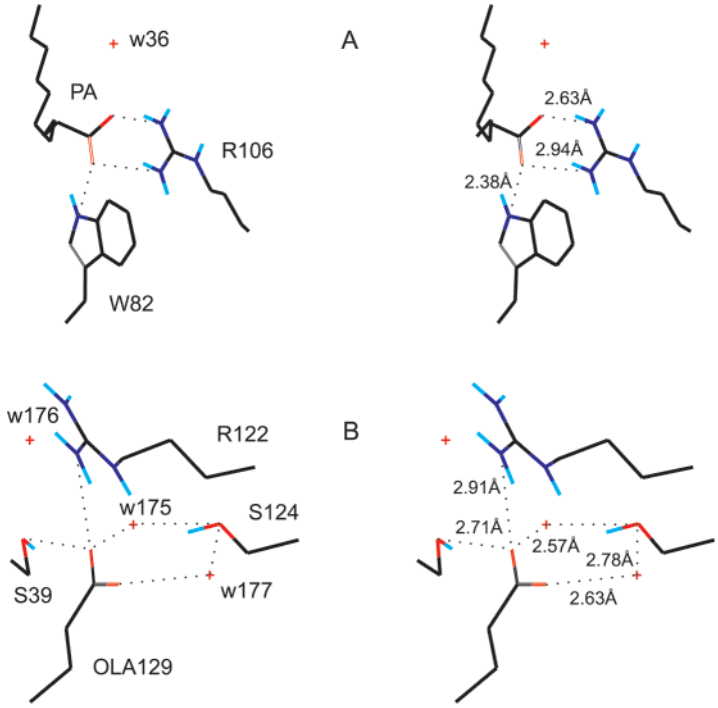

FIGURE 8: Stereoview comparison of the FA carboxylate headgroup binding pockets in IFABP (A) and LFABP (B). Coordinates were obtained from Protein Data Bank entries 2ifb (*26*) and 1lfo (*10*), respectively, and displayed with the SYBYL program. The lowercase w denotes the internal water molecules, numbered according to their respective PDB entries.

on the ^{13}C chemical shift time scale. Intermediate or rapid chemical exchange phenomena have been invoked previously to explain the observation of single carboxyl resonances in spectra of [*carboxyl*-^{13}C]OLA mixed with tissue-derived LFABP at 31 °C and pH >8.5 (*29*).

DISCUSSION

Molecular Environment of Fatty Acids Bound to LFABP. Both the X-ray structure (*10*) and the intermolecular $^1H-^1H$ NOEs measured by NMR methods (X.-M. Yang et al., unpublished experiments) provide evidence for at least two different OLA binding sites within the LFABP cavity. One carboxylate group (L_1) is buried deeply inside the cavity, and the other (L_2) lies near the protein surface and is exposed to solvent. At least six water molecules are observed within the ligand-binding cavity (*10*). These water molecules may provide a polar environment for the carboxyl end of the internal ligand (L_1), approximating that experienced by the carboxyl end of the ligand near the protein interface with the aqueous solvent (L_2).

Motional and Structural Basis for FA Exchange in LFABP Complexes. A recent NMR relaxation study shows that PA within the binding cavity of IFABP reorients twice as fast as the protein itself and over a wide angular range (*27*). Although no direct assessments of dynamic behavior have yet appeared for FAs within the liver-type protein, rapid reorientation is likely: this FABP has an unusually large cavity (*10*, *30*), small or unobservable prochiral α-methylene chemical shift dispersions, and small differences between carboxyl resonances corresponding to L_1 and L_2 in LFABP-bound PA and OLA. By comparison, PA complexed to IFABP displays prochiral α-methylene chemical shift dispersions that are 1 order of magnitude larger. Thus, fatty acid mobility may be one factor that facilitates exchange in FA−LFABP complexes.

Although hydrophobic interactions favor association of the protein-bound FA acyl chains, the electrostatic interactions deduced from the OLA−LFABP crystal structure suggest a rationale for enhanced FA exchange from complexes with this member of the protein family. The interaction between the internalized arginine and the FA carboxylate is likely to make a major enthalpic contribution to the binding of L_1 (OLA 129). In OLA−IFABP complexes, this carboxyl group is thought to be sequestered from the aqueous solvent over a wide pH range, whereas for the OLA−LFABP complex, the ionization behavior of bound ligand(s) is similar to that of bulk monomeric FA (*29*, *31*). This comparison can be better appreciated after examination of the respective X-ray structures, shown in Figure 8. In the liganded form of IFABP (Figure 8A), PA has a bidentate polar interaction with the R106 guanadino headgroup and is anchored further by interaction with W82. Many other FABPs utilize side chains from two arginines (and possibly water) to secure binding to the two oxygen atoms of the FA carboxylate (*10*). By

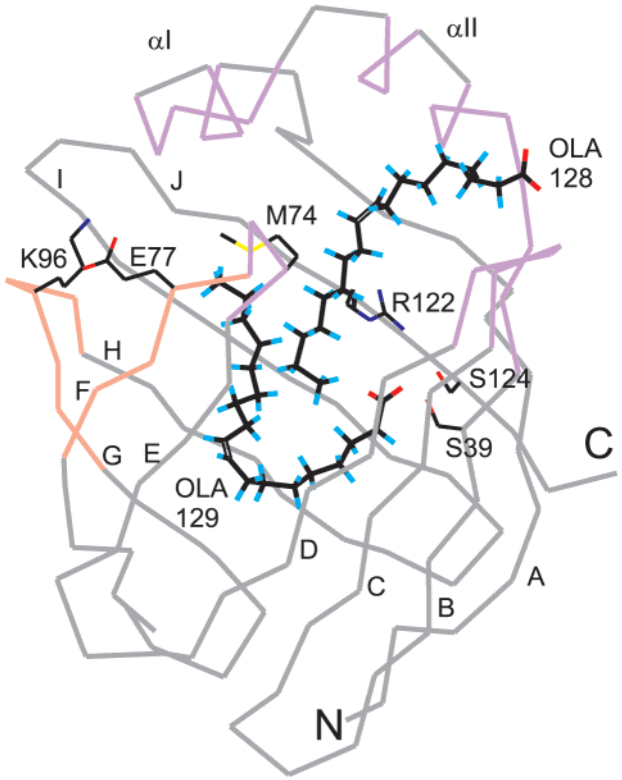

FIGURE 9: Representation of the LFABP X-ray structure (*10*) showing the two OLA ligands in the protein cavity. Drawn in purple is the purported primary lipid portal region common to all FABPs. Drawn in orange is the proposed secondary portal unique to LFABP, which may provide an escape route for the interior-bound FA molecule (see the text). Ten β-strands are denoted with the letters A−J, and the two α-helices are designated as αI and αII. Many of these structural features are confirmed in the holo-LFABP solution structure determined by NMR methods (X.-M. Yang et al., unpublished experiments).

contrast, OLA 129 interacts directly with LFABP by forming a strong hydrogen bond to a single oxygen, through interaction with R122 and S39 (Figure 8B). In this latter case, an intricate hydrogen-bonding system involving three internal water molecules (w175−w177) provides additional interaction but may also allow a measure of flexibility. S124 is connected to the fatty acid only indirectly through w175 and w177.

The X-ray structure of doubly liganded LFABP also allows for the possibility of direct L_1 exchange with bulk OLA, without the displacement of L_2. Direct L_1 egress may be possible because LFABP contains a unique gap in its hydrogen bond network adjacent to the loop between strands G and H (Figure 9) (*10*). This gap, which may be as large as 7.5 Å and has been proposed as a second portal region unique to LFABP (*10*, *30*, *32*), results from shortening the G and H strands and disrupting hydrogen bonds between the E and F strands and between the F and G strands, as compared to other FABPs. Although bulk solvent access to the interior is blocked by hydrophobic side chains, the proximity of the ω-CH_3 group of OLA 129 to this portal could allow for exit of an FA molecule, particularly if w175 displaces the single interaction anchoring the FA carboxylate oxygen to the protein.

OLA Exchange and Thermodynamic Properties of LFABP. The dissociation of oleate from LFABP has been examined

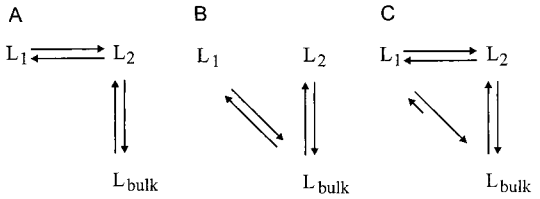

FIGURE 10: Possible exchange schemes for the OLA−LFABP complexes.

previously using fluorescence spectroscopy and titration calorimetry. The K_d values range from 0.009 to 0.2 μM for the primary site, and from 0.06 to 4.0 μM for the secondary site (*3*, *4*, *33*). The weaker binding parameters were determined by titration calorimetry, and the stronger binding estimates were obtained using a competing fluorescent fatty acid-binding protein. The calorimetric data suggest that entropy plays a substantial role in binding at both sites; the fluorescence measurements suggest that the binding is predominantly driven enthalpically for the first site but less so for the second one. The fluorescence studies indicate that the off-rates for both sites are on the order of 1 s^{-1}; the on-rates are diffusion-controlled for the first site and 1 order of magnitude slower for the second site (*34*, *35*).

Even in excess OLA, only two sets of resonances are observed in the NMR spectra at all accessible temperatures. One set of resonances has distinctive chemical shifts corresponding to L_1. The other set has chemical shifts that result from the averaging of L_2 and L_{bulk}. Thus, the interconversion of L_2 and L_{bulk} is fast on the chemical shift time scale and cannot be measured in the *z*,*z*-exchange experiment. LFABP can solubilize up to 8 equiv of oleate, yet only two ligands were identified clearly in the X-ray structure. A four-carbon segment was located in the electron density map near the beginning of helix αI, suggesting a possible binding site for a third oleate. In the presence of LFABP, excess OLA does not form bilayers and the solution remains optically clear, even though free OLA at this bulk concentration and pH is known to form a turbid bilayer solution (*14*). The fast exchange observed between L_2 and L_{bulk} suggests that L_{bulk} is solubilized near the primary portal region of LFABP. Thus, rapid exchange of L_2 with the bulk may compete effectively with bilayer formation.

Schemes for Fatty Acid Exchange. Published X-ray data depict the OLA−LFABP complex as a two-ligand system (Figure 9**)**, in which the hydrophobic packing of OLA 128 and 129 suggests that binding of L_2 (OLA 128) depends on the presence of L_1 (OLA 129) (*10*). This hypothesis is supported by our observation that NMR resonances arising from OLA at the L_1 site are shifted significantly depending on whether the L_2 site is occupied (Figure 5), presumably because the two ligands experience hydrophobic interactions rather than occupying separate, independent pockets of the protein-binding cavity. Possible exchange schemes for these ligands are depicted in Figure 10. These scenarios assume that exchange is rapid between L_2 and the unbound aqueous (bulk) ligand, consistent with NMR spectra in which at most two resonances are observed for each chemical moiety upon addition of 1−8 equiv of OLA, and that the slow exchange rate of ~54 s^{-1} measured in the *z*,*z*-exchange experiment is determined by processes involving L_1, i.e., exchange with L_2 within the cavity or direct exchange with L_{bulk}.

In Scheme A, ligands L_1 and L_2 exchange with each other within the cavity, and L_2 also undergoes exchange with bulk OLA. The internal exchange process then corresponds to the 54 s^{-1} value for k_{ex} measured in the *z,z*-exchange experiment; i.e., it occurs much more slowly than the L_2 exchange with bulk OLA. In Scheme B, exchange of L_1 and L_2 within the cavity does not occur, but both ligand molecules exchange with the bulk OLA. Exchange of L_1 through the main portal requires dissociation of L_2 from the protein complex; thus, exchange of L_1 with bulk OLA would occur from the singly liganded LFABP species. Under our experimental conditions, the population of singly liganded species is very low and exchange broadening effects should be minimal. Thus, the measured exchange rate constant cannot reflect stepwise dissociation of L_1 and L_2. If a second portal allows direct exchange of L_1 with L_{bulk}, without prior dissociation of L_2, the measured exchange rate would correspond directly to this kinetic process. In Scheme C, intracavity exchange occurs between L_1 and L_2 and both ligands also exchange directly with L_{bulk}. Scheme C combines both schemes A and B, and the measured exchange rate constant could correspond to either intracavity exchange or direct exchange of L_1 with bulk OLA through the second portal. These experiments cannot distinguish between intracavity exchange between L_1 and L_2 and direct exchange of L_1 with bulk OLA, because the fast exchange of L_2 and bulk OLA yields a single averaged resonance for the latter two species.

Functional Implications. The ability of LFABP to bind two fatty acid molecules within its cavity and solubilize up to 8 equiv of FA (*31*, *36*, *37*) is unprecedented in the FABP family, although several related phenomena have been reported. For instance, a plant nonspecific lipid transfer protein has been shown to bind two molecules of lysomyristoylphosphatidylcholine (*38*), and a bile acid-binding protein has been reported to bind 2 equiv of bile acid with weak intrinsic affinity but high cooperativity (D. P. Cistola, personal communication). Binding of the first ligand to LFABP may trigger expansion of the protein cavity and has been proposed to make available a hydrophobically compatible face for binding of the second ligand (*10*). The data presented herein also suggest that the protein permits facile exchange of the second ligand with the bulk pool of FA molecules.

LFABP is also atypical among the FABPs because it transfers FA to membranes via a diffusion-mediated rather than collision-mediated mechanism (*8*, *9*, *39*). The binding stoichiometry and exchange schemes deduced for OLA−LFABP complexes, along with crystal and solution-state structural data, suggest a molecular hypothesis to describe this transfer process. Transport of L_2 (OLA 128) into the aqueous milieu occurs rapidly by chemical exchange with a large pool of bulk solubilized OLA, whereas release of L_1 (OLA 129) occurs on a slower time scale, either through the mediation of L_2 or by direct escape through a second portal. Bulk OLA may be associated loosely with the protein and shuttled rapidly in and out of the cavity. The ability of LFABP to accommodate two ligands within an expanded protein cavity produces a complex for which interactions with the FAs are weakened and interstrand gaps offer the potential for FA escape through more than one mechanism.

Thus, LFABP has a capability for facile release of FA molecules, which may occur even in the absence of a collision-driven "pull" from acceptor membranes. Alternatively, a modest level of collisional FA transfer may occur from LFABP to membranes under some circumstances. In particular, we have observed that vesicles containing the anionic phospholipid cardiolipin exhibit 2-fold faster rates of transfer from LFABP than zwitterionic vesicles (*8*), and Wilton and co-workers (*40*) showed that LFABP−membrane interactions occur under low-ionic strength conditions. These results suggest the possibility of electrostatic interactions between the protein and membranes that could serve to further depopulate the ligand-binding cavity.

ACKNOWLEDGMENT

We gratefully acknowledge Drs. Alan Kleinfeld and Ron Ogata for providing the rat LFABP cDNA. For assistance with the implementation and analysis of NMR experiments, we thank Drs. Lewis Kay and Ranjith Muhandiram (pulse sequences), Frank Delaglio (NMRPipe), and Bruce Johnson (NMRView).

REFERENCES

1. Glatz, J. F. C., and van der Vusse, G. J. (1996) *Prog. Lipid Res. 35*, 243−282.
2. Banaszak, L., Winter, N., Xu, Z., Bernlohr, D. A., Cowan, S., and Jones, T. A. (1994) *Adv. Protein Chem. 45*, 89−151.
3. Richieri, G. V., Ogata, R. T., and Kleinfeld, A. M. (1994) *J. Biol. Chem. 269*, 23918−23930.
4. Rolf, B., Oudenampsen-Kruger, E., Borchers, T., Faergeman, N. J., Knudsen, J., Lezius, A., and Spener, F. (1995) *Biochim. Biophys. Acta 1259*, 245−253.
5. Bass, N. M. (1988) *Int. Rev. Cytol. 3*, 143−184.
6. Storch, J. (1993) *Mol. Cell. Biochem. 123*, 45−53.
7. Vincent, S. H., and Muller-Eberhard, U. (1985) *J. Biol. Chem. 260*, 14521−14528.
8. Hsu, K. T., and Storch, J. (1996) *J. Biol. Chem. 271*, 13317−13323.
9. Storch, J., and Thumser, A. E. A. (2000) *Biochim. Biophys. Acta 1486*, 28−44.
10. Thompson, J., Winters, N., Terwey, D., Bratt, J., and Banaszak, L. (1997) *J. Biol. Chem. 272*, 7140−7150.
11. Cistola, D. P., Sacchettini, J. C., Banaszak, L. J., Walsh, M. T., and Gordon, J. I. (1989) *J. Biol. Chem. 264*, 2700−2710.
12. Nemecz, G., Jefferson, J. R., and Schroeder, F. (1991) *J. Biol. Chem. 266*, 17112−17123.
13. Wang, H., He, Y., Hsu, K. T., Magliocca, J. F., Storch, J., and Stark, R. E. (1998) *J. Biomol. NMR 12*, 197−199.
14. Cistola, D. P., Atkinson, D., Hamilton, J. A., and Small, D. M. (1986) *Biochemistry 25*, 2804−2812.
15. Lowry, O. H., Rosenbrough, N. J., Farr, A. L., and Randall, R. J. (1951) *J. Biol. Chem. 193*, 265−278.
16. Ohnishi, S. T., and Barr, J. K. (1978) *Anal. Biochem. 86*, 193−200.
17. Vuister, G. W., and Bax, A. (1992) *J. Magn. Reson. 98*, 428−435.
18. Yamazaki, T., Nicholson, L. K., Torchia, D. A., Wingfield, P., Stahl, S. J., Kaufman, J. D., Eyermann, C. J., Hodge, C. N., Lam, P. Y. S., Ru, Y., Jadhav, P. K., Chang, C.-H., and Weber, P. C. (1994) *J. Am. Chem. Soc. 116*, 10791−10792.
19. Smallcombe, S. H., Patt, S. L., and Keifer, P. A. (1995) *J. Magn. Reson., Ser. A 117*, 295−303.
20. Patt, S. L. (1992) *J. Magn. Reson. 96*, 94−102.
21. Farrow, N. A., Zhang, O., Forman-Kay, J. D., and Kay, L. E. (1994) *J. Biomol. NMR 4*, 727−734.
22. Montelione, G. T., and Wagner, G. (1989) *J. Am. Chem. Soc. 111*, 3096−3098.
23. Wider, G., Neri, D., and Wuthrich, K. (1991) *J. Biomol. NMR 1*, 93−98.
24. Delaglio, F., Grzesiek, S., Vuister, G. W., Zhu, G., Pfeifer, J., and Bax, A. (1995) *J. Biomol. NMR 6*, 277−293.

25. Johnson, B. A., and Blevins, R. A. (1994) *J. Biomol. NMR 4*, 603−614.
26. Sacchettini, J. C., Gordon, J. I., and Banaszak, L. (1989) *J. Mol. Biol. 208*, 327−339.
27. Zhu, L., Kurian, E., Prendergast, F. G., and Kemple, M. D. (1999) *Biochemistry 38*, 1554−1561.
28. Martin, G. E., Spitzer, T. D., Crouch, R. C., Luo, J.-K., and Castle, R. N. (1992) *J. Heterocycl. Chem. 29*, 577−582.
29. Cistola, D. P., Walsh, M. T., Corey, R. P., Hamilton, J. A., and Brecher, P. (1988) *Biochemistry 27*, 711−717.
30. Thompson, J., Ory, J., Reese-Wagoner, A., and Banaszak, L. (1999) *Mol. Cell. Biochem. 192*, 9−16.
31. Cistola, D. P., Sacchettini, J. C., Banaszak, L. J., Walsh, M. T., and Gordon, J. I. (1989) *J. Biol. Chem. 264*, 2700−2710.
32. Thompson, J., Reese-Wagoner, A., and Banaszak, L. (1999) *Biochim. Biophys. Acta 1441*, 117−130.
33. Miller, K. R., and Cistola, D. P. (1993) *Mol. Cell. Biochem. 123*, 29−37.
34. Richieri, G. V., Ogata, R. T., and Kleinfeld, A. M. (1996) *J. Biol. Chem. 271*, 31068−31074.
35. Richieri, G. V., Ogata, R. T., Zimmerman, A. W., Veerkamp, J. H., and Kleinfeld, A. M. (2000) *Biochemistry 39*, 7197−7204.
36. Lowe, J. B., Sacchettini, J. C., Laposata, M., McQuillan, J. J., and Gordon, J. I. (1987) *J. Biol. Chem. 262*, 5931−5937.
37. Nemecz, G., Jefferson, J. R., and Schroeder, F. (1991) *J. Biol. Chem. 266*, 17112−17123.
38. Charvolin, D., Douliez, J.-P., Marion, D., Cohen-Addad, C., and Pebay-Peyroula, E. (1999) *Eur. J. Biochem. 264*, 562−568.
39. Thumser, A. E. A., and Storch, J. (2000) *J. Lipid Res. 41*, 647−656.
40. Davies, J. K., Thumser, A. E., and Wilton, D. C. (1999) *Biochemistry 38*, 16932−16940.
41. Shaka, A. J., Barker, P. B., and Freeman, R. (1985) *J. Magn. Reson. 64*, 547−552.
42. Bax, A., and Pochapsky, S. S. (1992) *J. Magn. Reson. 99*, 638−643.
43. Marion, D., Ikura, M., Tschudin, R., and Bax, A. (1989) *J. Magn. Reson. 85*, 393−399.

BI011914G